The Journal of Chemical Physics

RESEARCH ARTICLE | NOVEMBER 04 2025

Fine tuning of long-range interactions to describe the binding of adamantane and diamantane derivatives to a Cucurbit[7]uril-based synthetic receptor: Insights from metadynamics simulations

Special Collection: Michele Parrinello Festschrift

Amal Vijay ; Giacomo Salvadori ; Frank Biedermann ; Giulia Rossetti ; Paolo Carloni ; Davide Mandelli

J. Chem. Phys. 163, 175102 (2025)
https://doi.org/10.1063/5.0288329

The Journal of Chemical Physics ARTICLE pubs.aip.org/aip/jcp

Fine tuning of long-range interactions to describe the binding of adamantane and diamantane derivatives to a Cucurbit[7]uril-based synthetic receptor: Insights from metadynamics simulations

Cite as: J. Chem. Phys. 163, 175102 (2025); doi: 10.1063/5.0288329
Submitted: 30 June 2025 • Accepted: 10 October 2025 •
Published Online: 4 November 2025

Amal Vijay,[1] Giacomo Salvadori,[1] Frank Biedermann,[2] Giulia Rossetti,[1,3,4] Paolo Carloni,[1,5,6,a)] and Davide Mandelli[1,a)]

AFFILIATIONS

[1] Institute of Neuroscience and Medicine (INM-9), Computational Biomedicine, Forschungszentrum Jülich, 52428 Jülich, Germany
[2] Institute of Nanotechnology (INT), Karlsruhe Institute of Technology(KIT), Hermann-von-Helmholtz Platz 1, 76344 Eggenstein-Leopoldshafen, Germany
[3] Department of Neurology, University Hospital RWTH Aachen University, 52074 Aachen, Germany
[4] Jülich Supercomputing Centre (JSC), Forschungszentrum Jülich GmbH, Jülich 52428, Germany
[5] Department of Physics, RWTH Aachen University, 52074 Aachen, Germany
[6] JARA-Brain Institute Molecular Neuroscience and Neuroimaging (INM-11), Forschungszentrum Jülich, 52428 Jülich, Germany

Note: This paper is part of the JCP Special Topic, Michele Parrinello Festschrift.
[a)] **Authors to whom correspondence should be addressed:** p.carloni@fz-juelich.de and d.mandelli@fz-juelich.de

ABSTRACT

High-affinity host–guest systems, such as Cucurbit[n]uril (CBn) macrocycles, are vital across various scientific and technological fields—such as targeted drug delivery, smart (self-healing) materials, sensitive biosensors, and molecular diagnostics—due to their exceptional molecular recognition capabilities. Molecular simulation (MS)-based predictions of ligands' binding poses and affinities on the macrocycles would greatly help optimize such host–guest systems. Yet, the poor accuracy of force fields (FFs) for these synthetic receptors has limited the applicability of MS thus far. Here, we demonstrate that incorporating electron density-derived Lennard-Jones parameters and charges into FFs can drastically improve the accuracy of free-energy calculations for these systems. As a test case, we focus on five adamantane derivatives and two diamantane derivatives in complex with one of the macrocycles, CB7. Our free energies of binding, calculated via multiple-walker well-tempered funnel metadynamics, turned out to be in fair agreement with the experiment for all the adamantane molecules. For the larger diamantane molecules, we still observe a discrepancy with experiments, which calls for deeper investigation. Overall, the calculations also provide insights into the binding mechanism and the role of the solvent. In particular, the chemical structures of the ligands and the ion strength play an important role in the binding process.

INTRODUCTION

High-affinity synthetic host–guest complexes, including Metabolite Binding Synthetic Receptors (MSRs), have become indispensable in modern supramolecular chemistry, enabling precise molecular recognition through noncovalent inclusion binding. These systems can form ultra-stable complexes—with binding constants often in the 10^{12}–$10^{15}M^{-1}$[1–6] range, even surpassing the avidin–biotin benchmark—which underpins their broad utility across diverse fields. In biomedical science, for example, host–guest macrocycles are exploited in drug delivery to encapsulate and protect therapeutics, improving drug stability and efficacy (e.g., prolonging antibiotic shelf-life via photostabilization), while also enabling targeted delivery and controlled release profiles for pharmaceuticals.[7–9] Likewise, in molecular diagnostics and imaging, the high selectivity and affinity of host–guest pairs allow for highly sensitive detection strategies.[10–13] In materials science, incorporating high-affinity host–guest interactions into polymers and nanoparticles has given rise to "smart" materials—such as responsive hydrogels, supramolecular assemblies, and even molecular machines—that undergo controlled changes in response to chemical or physical stimuli.[14–18] Particularly interesting are the Cucurbit[n]uril (CBn, where n = 5, 6, 7, 8, 10, 14) macrocycles whose deep, centrally positioned cavities enable them to accommodate a diverse range of guest molecules with high stability.[19–23] In particular, CB7 [Fig. 1(a)] exhibits high selectivity for adamantane and diamantane derivatives, some of which are shown in Figs. 1(b) and 1(c), as the adamantane core fits almost ideally within the cucurbituril cavity. Adamantane-containing molecules are known for their low molecular strain, high stability, hydrophobicity, and ease of donor–acceptor functionalization, serving as rigid scaffolds that enable strong binding to CB7 hosts.[23]

Accurate predictions of ligand binding affinities for CB7 (as well as for other synthetic hosts) by atomistic simulations[24,25] would greatly help in the optimization of such systems for medical applications. Unfortunately, this has been severely limited by inaccuracies of free energy methods, including alchemical free energy calculations and enhanced sampling techniques, combined with force fields, such as GAFF,[26] CGenFF,[27] OPLS,[28] and the Open Force Field[29,30] force fields (Table S1).[31–33] The role of the water models, such as TIP3P,[34] TIP3P-FB,[35] SPC/E,[36] TIP4P,[34] and OPC3,[37] has also been shown to affect the predictions and energetics.[38,39] Incorporating QM-derived data to refine partial charges and bonded parameters improved the accuracy for a variety of MSRs (including CB7), yet differences with experiment are still sizable[40–43] (see Tables S1 and S2 of the supplementary material). Overall, these limitations might prevent the exploitation of computational chemistry for the development of new and more potent MSRs.

Here, we develop a modified force field (*modified-FF* from now on) that incorporates nonbonded Lennard-Jones (LJ) parameters and partial charges derived from molecular electron density obtained using accurate density functional theory (DFT) QM calculations. This work is partly inspired by a recent paper by González *et al.*,[44] where the authors derived nonbonded force field parameters by partitioning molecular electron density obtained from QM/MM calculations, showing improved accuracy of ligand binding affinities toward aromatic and adamantane core-based molecules for CB7.[44] *Modified-FF* based, multiple walkers,[45] well-tempered funnel metadynamics[24] free energy calculations on seven selected positively charged, negatively charged, and neutral adamantane and diamantane derivatives (see Fig. 1) are then carried out in the presence and absence of salt concentration. This allowed us to investigate the impact on the binding free energy across different ligand charges and with different ionic strength conditions, which is known to play an important role in the binding.[46–50]

Experimentally, it has been observed that positive ligands exhibit stronger binding affinities to CB7 than neutral and negatively charged ligands (Table I), highlighting the role of electrostatic attraction in stabilizing host–guest interactions. Among the positively charged ligands, **5** (Fig. 1) exhibits higher binding affinity than **4** and **6**, pointing to the role of the protonated amine groups present in **5**: their substitutions to adamantane may introduce steric

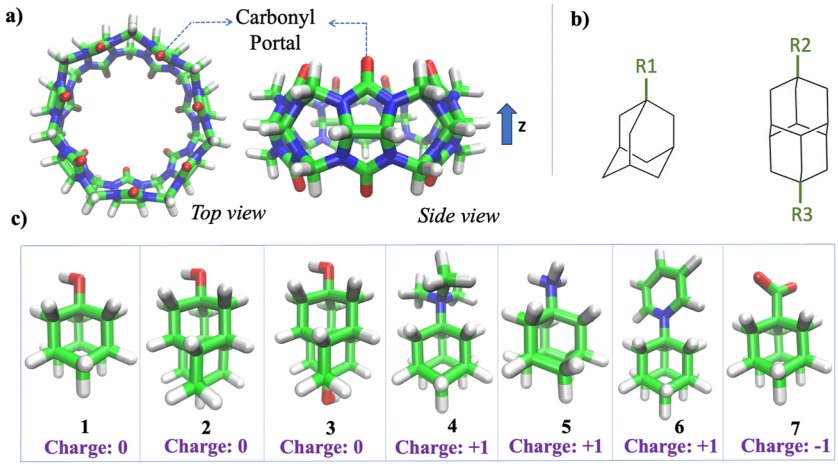

FIG. 1. (a) Top and side views of CB7 aligned along the z-axis. A representative atom at the carbonyl portal is indicated by an arrow. (b) Core structures of adamantane and diamantane derivatives binding to CB7 (R1 = –OH, $–COO^-$, NH_3^+, $C_5H_5N^+$, and $N(CH_3)_3^+$, R2 = –H or –OH R3 = –OH). (c) 3D structures and charges of individual adamantane and diamantane molecules, along with their corresponding IDs.

TABLE I. Experimental binding free energy (ΔG_{bind}^{Expt}) of the studied molecules at 0 and 50 mM ion concentrations. Ligand labeling as in Fig. 1(c).

Molecule ID	ΔG_{bind}^{Expt} (kcal/mol)	
	0 mM	50 mM
1	−14.1 ± 0.2,[46] −14.2 ± 0.4[47]	...
2	−9.3 ± 0.4[47]	...
3	−9.6 ± 0.4[47]	...
4	...	−16.7 ± 0.1[48]
5	−19.4 ± 0.1[46]	−17.2 ± 0.1[48]
6	...	−16.8 ± 0.8[48]
7	...	−11.6 ± 0.1[48]

penalties or reduce encapsulating ability in **4** and **6**. The neutral ligand **1** binds stronger than the neutral ligands **2** and **3** (Table I). This can be attributed to its mono-adamantane core and optimal size complementarity with CB7's cavity. Taken together, the data underscore that while positive charge significantly enhances binding, its influence is affected by steric accessibility and size compatibility with the CB7 cavity.

Anticipating our results, the binding affinity predictions across all ligands turn out to be closer to experiments than those based on the standard General AMBER Force Field (GAFF),[26] performed here with the same setup. However, quantitative agreement is observed only in the case of adamantane derivatives. The shape of the multidimensional free energy landscape for the latter remains mostly unchanged on passing from the GAFF to the *modified-FF* predictions, indicating that the (un)binding mechanism is not affected by the choice of the force fields.

METHODS

Systems

We considered the seven ligands in Fig. 1, for which experimental binding affinities are available (Table I). The molecular geometries of the ligands were constructed and optimized *in vacuo* with the MMFF94 force field—as implemented in the Avogadro software[51] (version 1.2.0)—and subsequently refined in the DFT QM calculations at the HF/6-31G(d,p) level of theory, using the Psi4[52] package. For CB7, quantum mechanically optimized atomic coordinates of CB7 were taken from Ref. 47. The CB7/ligand complexes were prepared by positioning the ligands at the center of the CB7 cavity such that the substitutions [R1, R2, and R3 in Fig. 1(b)] are aligned along the +Z direction. The systems were solvated using ~5000 water molecules. For charged ligands [**4–7** in Fig. 1(c)], additional Na^+/Cl^- ions were added in order to maintain neutrality of the system. The systems were prepared either without or with an ion concentration of 50 mM (Na^+ and Cl^-). Each system contained ~15 200 atoms within a cubic box of edge ~5.4 nm.

Force fields

We have utilized three force fields for both CB7 and ligands:

(a) The GAFF[26], which was built using the antechamber[53] module of AMBERTOOLS. Semi-empirical AM1-BCC partial charges[54] were assigned to both CB7 and each of the selected guest molecules. The resulting topology and coordinates for each entity were then converted to GROMACS format using ACPYPE.[55] We have also carried out a test case study using GAFF[26] with RESP and GAFF2[26] with AM1-BCC for molecules **1** and **2**, the results of which are discussed in Secs. SVI–VII of the supplementary material. We note that the ABCG2 charge model[56] has been suggested as an alternative charge model for GAFF2. Here, we only considered GAFF2 in combination with AM1-BCC charges.

(b) The *modified-FF*, which differs from GAFF for (i) the Lennard-Jones (LJ) parameters and (ii) the charges. The LJ well-depth (ε) and van der Waals radius (σ) parameters were derived using a quantum mechanics to molecular mechanics (QM-to-MM) mapping strategy based on the atoms-in-molecule (AIM)[57] analysis. The molecular electron density is partitioned into atomic densities using the MBIS[58] based AIM partitioning scheme implemented in QUBEKit,[58–60] based on a QM calculation at the HF/6-31G(d,p) level of theory with a continuum solvation model. The latter was implemented to incorporate the molecular environment of the solvent. This approach was carried out for each ligand and a monomeric building block of CB7. The dispersion (*C6*) coefficients are derived from atomic electron densities following the Tkatchenko–Scheffler method.[61] The repulsive term (*C12*) was obtained following the method of Refs. 57, 59, and 60. The *C6* and *C12* coefficients are automatically transformed into LJ parameters σ and ϵ by QUBEKit and used to generate GROMACS topology files. The main difference in our FF is the lowering of the ε parameter, which is found to be halved with respect to the original GAFF (Fig. S1). We note that lowering ε of both guest and host simultaneously weakens the guest–host and guest- and host-solvent interactions, making the net effect on binding affinity nontrivial and not predictable *a priori*. (ii) The charges were computed using the RESP[62] methods at the B3LYP/6-311++G(d,p) level of theory. Long-range solvation effects were incorporated using the polarizable continuum model (PCM).[63–65] We chose B3LYP/6-311++G(d,p) over the HF/6-31G(d,p) for charge derivation due to its advantages in reproducing key electrostatic properties.[66] B3LYP incorporates electron correlation missing in HF and better captures electrostatic potentials, dipole moments, and polarization behaviors crucial to accurate partial charges. Benchmarking studies confirm that HF underperforms in these regards.[66]

On the other hand, HF/6-31G(d,p) was employed for deriving Lennard-Jones (LJ) parameters. This follows the QUBEKit framework,[59] where HF-level AIM calculations are used for LJ parameter extraction. We adhered to this protocol to ensure compatibility with existing parameterization pipelines. To test the dependence of the LJ parameterization on the level of theory, we have also performed parameterization at the B3LYP/6-311++G(d,p) level for ligand 1. The results are reported in Fig. S2, showing negligible differences compared to HF/6-31G(d,p).

(c) To single out the effect of the LJ when comparing our results with the GAFF, calculations were carried out also with the *modified-FF* in combination with the AM1-BCC charges.

For water, we used the TIP3P[34] model. Changing the water model, however, turned out not to impact significantly the results (see Table S3). For the ions, we used the parameters developed by Joung and Cheatham.[67]

Details of the simulations

Periodic boundary conditions were applied in all directions. Long-range electrostatic interactions were treated using the Particle Mesh Ewald (PME) method.[68] A cutoff distance of 1.0 nm was applied to both vdW and the real part of the electrostatic interactions. All bonds involving hydrogen atoms were constrained using the LINCS algorithm.[69] A 2 fs integration time step was used.

Molecular dynamics equilibration of the systems

The systems underwent energy minimization using the steepest descent method for 50 000 steps, followed by 10 ns NVT MD (T = 300 K) using the velocity rescaling thermostat.[70] The systems then underwent 20 ns NPT MD, employing the velocity rescaling thermostat[70] and Berendsen barostat[71]. A time constant of 0.1 ps was used for the thermostat, while a time constant of 2.0 ps was used for the barostat. In NVT and NPT simulations, the target temperature was 300 K, while the target pressure was 1 atm. All the systems stayed in the bound configuration during the equilibration.

Free energy via funnel metadynamics[24]

The simulations were performed in the NPT ensemble. Constant temperature (300 K) and pressure (1 atm) conditions were achieved by coupling the systems with the velocity rescaling thermostat[70] and the Parrinello–Rahman barostat,[72] respectively. A time constant of 0.1 ps was used for the thermostat, and a time constant of 2.0 ps was used for the barostat.

The free energy was calculated as a function of two collective variables (CVs):

(a) *DistZ*: the distance between the center of mass (COM) of the host and the COM of the guest, projected along the z-axis of the host (Fig. 2). The COM was computed using only heavy atoms.
(b) The *binding mode angle* (θ). This CV characterizes the orientation of the guest relative to the host [Fig. 2(b)]. It is defined as the angle between the z-axis and the vector connecting the COM of the bottom and top part of the adamantane core. The heavy atoms used to define the top and bottom parts are shown in Fig. 2(b).

DistZ accelerates the displacement of the guest moving in and out of the CB7 cavity, while θ accelerates the guest's orientation relative to the z-axis. It also accounts for any steric hindrance that may affect the guest's entry into or exit from the cavity. Moreover, we also observed that using both *DistZ* and θ as CVs enhances binding/unbinding transitions compared to using only *DistZ*, potentially leading to faster convergence in the current protocol. Harmonic upper-wall and lower-wall restraints with a spring constant of 50 000 kJ/mol were applied to the *DistZ* CV at 2.2 and −2.2 nm, respectively, to ensure the efficient exploration of both bound and unbound states.

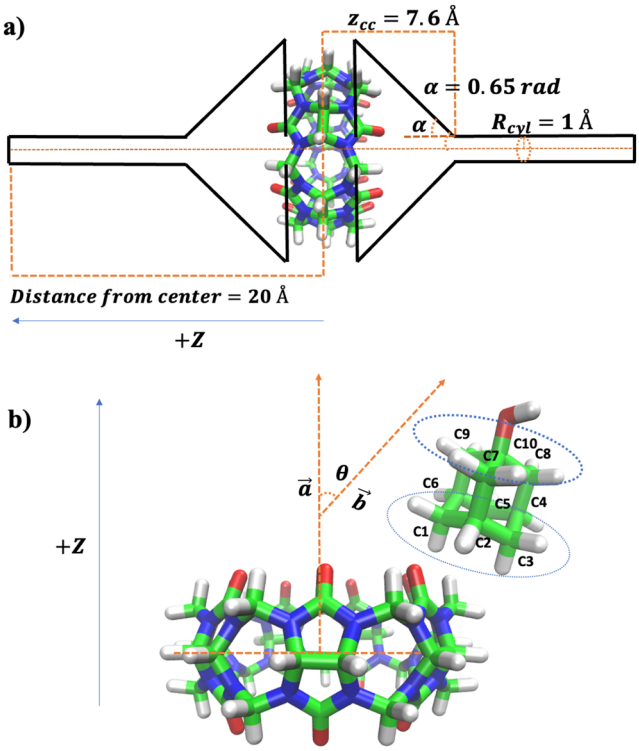

FIG. 2. (a) Representation of the binding/unbinding axis (z), funnel parameters, and the shape of the funnel restraint with respect to CB7, as described in Eq. (1). The figure also illustrates the shape and location of the funnel restraint used in funnel metadynamics simulations. (b) Representation and description of the CV θ, which defines the binding mode of molecule 1 toward CB7. The vector $\vec{a}$ is aligned with the reference z-axis, while the vector $\vec{b}$ connects the COM of the bottom carbon atoms (C1, C2, C3, C4, C5, and C6) in ligand 1 to the top carbon atoms (C7, C8, C9, and C10).

Funnel metadynamics[24] was started from the final structures obtained after equilibration. The method uses a funnel-shaped restraint potential to restrict the motion of a ligand (un)binding from its guest to a reduced region of phase space in order to speed up the transitions. The following parameters were used in our simulations to construct the funnel: z_{cc} = 7.6Å, R_{cyl} = 1Å, and α = 0.65 rad (see Fig. 2 for definitions). Due to the symmetry of the CB7 host along the binding axis, we applied a double-sided funnel potential extending outward in both the +Z and −Z directions from its center.[39,73] This setup allows the ligand to (un)bind (from) to the cavity of CB7 from both sides, avoiding possible biases in the free energy estimation.

We define (i) the bound state as the global minima of the computed 1D free energy surface as a function of *DistZ* and (ii) the unbound states as those associated with $|DistZ| > 1.5$ nm (that is, featuring no direct ligand/receptor interactions), where the 1D free energy surface reaches a plateau. The difference in free energy between the bound and unbound states as directly extracted from the 1D free energy surface defines the computed binding free energy ΔG_{metad}. Using the 2D free energy surface to extract ΔG_{metad} led

to the same results. The effect of the funnel potential can be rigorously taken into account to compute the absolute binding free energy ΔG_{bind} by adding an analytical correction, ΔG_{funnel},

$$\Delta G_{bind} = \Delta G_{metad} + \Delta G_{funnel}. \quad (1)$$

The funnel correction term is given by

$$\Delta G_{funnel} = -\frac{1}{\beta} \ln\left(\pi R_{cyl}^2 C^0\right), \quad (2)$$

where C^0 = 1/1660 Å^{-3} is the standard concentration and πR^2_{cyl} is the cross section of the cylindrical part of the funnel-shaped restraint potential. Using our setup, the funnel correction is equal to ΔG_{funnel} = 3.8 kcal/mol.

In all simulations, we have utilized a well-tempered version of metadynamics[74] combined with the multiple-walker[45] approach, which enhances sampling efficiency, accelerates convergence, and improves the overall performance of the simulation. Gaussian kernels are added in the 2D CV space every picosecond, with an initial Gaussian height of 1 kJ/mol. The Gaussian widths were set to 0.1 nm and 0.15 rad, respectively, for *DistZ* and θ. A bias factor of 20 was employed.

We performed multiple-walker, well-tempered metadynamics simulations using 20 walkers, each run for 50 ns, corresponding to a cumulative (20 walker × 50 ns/walker) = 1000 ns of effective sampling. The time evolution of biased CVs during these simulations is shown in Figs. S3–S8 of the supplementary material.

The walkers share a common bias potential such that at any given time, the free energy surface (FES) reflects the combined bias accumulated from all walkers. The FES in the CV space was reconstructed directly from the deposited bias using the standard *sum_hills* procedure as implemented in PLUMED 2.8,[75] which integrates contributions from all the walkers. We monitored the free energy difference $\Delta G_{metad}(t)$ between the bound and the unbound states as a function of simulation time for all the systems to ensure the convergence of free energy calculations. The convergence plots are shown in Fig. S9 of the supplementary material.

Binding affinities (ΔG_{bind}) have been computed using the time-averaged value of $\Delta G_{metad}(t)$ obtained considering the last portion of the trajectory, where ΔG_{metad} reaches a plateau. For all the ligands, this corresponds to the last (15 ns × 20 walkers) = 300 ns of effective sampling (see Fig. S9). The reported uncertainties on ΔG_{bind} are standard deviations computed using values of ΔG_{metad} extracted at equally spaced intervals Δt during the last 300 ns of effective sampling. For each molecule, Δt was chosen to obtain a fully converged estimate of the standard deviation (see Fig. S10).

All simulations were conducted using GROMACS 2022[76] patched with PLUMED 2.8[75] to perform the metadynamics simulations.

RESULTS AND DISCUSSION

The free energy surface associated with ligands' binding to the receptor was calculated using multiple walker funnel metadynamics,[24] using GAFF with charges calculated at the AM1-BCC[54] level of theory [GAFF (AM1-BCC) hereafter], our *modified-FF*, which differs from GAFF for the LJ parameters and for the use of RESP[62] charges [*modified-FF* (RESP)]. To identify the sole effect of the modified LJ parameters on the predictions, we also performed simulations using a FF, which differs from GAFF only for the LJ parameters [*modified-FF* (AM1-BCC)].

We first discuss the free energy surfaces obtained using the *modified-FF* (RESP) at concentrations consistent with those of available experimental results. These are reported in Fig. 3 together with the representative snapshots of the bound-state conformations.

The landscape reveals distinct binding characteristics for each CB7–guest complex. **1** and **5**, which contain adamantane core, exhibit well-defined minima near the center of the cavity (*DistZ* ≈ 0 nm), with broad accessibility across the orientation angle ($\theta \approx 0.0$–0.6 and 2.4–3.1 rad), suggesting stable, slightly tilted binding poses and moderate orientational flexibility inside CB7. This indicates multiple accessible binding orientations near the cavity center. In contrast, **2** and **3**, which contain diamantane cores, show shallow and more confined minima, with broad high-energy barrier regions (highlighted red color in the free energy landscape) along the θ axis, reflecting steric hindrance and restricted orientation flexibility due to their bulky substitutions. Similarly, **4** and **6**, which contain adamantane cores with bulky substituents, exhibit narrow, offset minima (*DistZ* ≈ 0.13–0.20 nm) and wide barriers in θ space, also suggesting limited flexibility of the ligand in the cavity imposed by the restrictions caused by side groups. **7** contains the adamantane core. Although it has less bulky substitutions, it shows distinct high-energy barriers near the entrance region (*DistZ* ≈ ±0.5 nm), likely arising from its negatively charged carboxylate group causing repulsions to the carbonyl groups of CB7. Overall, guests with bulkier cores or substituents (**2**, **3**, **4**, and **6**) display more flatter barrier regions in the θ CV space, whereas smaller or more flexible guests (e.g., **1** and **5**) exhibit broader accessible basins and lower energy barriers in the θ CV space. These results highlight the role of steric and electrostatic factors in determining binding mode diversity within CB7.

We have also performed test calculations using the GAFF in combination with the RESP charges computed at the B3LYP level of theory. The results (discussed in Sec. SVI of the supplementary material) show that the results of GAFF-based binding affinity predictions using different charge models are generally system dependent, as previously observed.[77,78] Overall, as shown in Fig. S11 and Table. S4, the predictions of our *modified-FF* (RESP) potential remain the closest to experiments. We have also performed tests using the new GAFF2[26] force field in combination with the AM1-BCC. The results (discussed in Sec. SVII of the supplementary material) show that the change in parameters between GAFF and GAFF2 affect the computed energetics in a ligand-dependent manner (Fig. S12 and Table S5) as already reported in previous studies.[79,80] In particular, for the two ligands considered, the use of GAFF2 does not lead to significant improvements in the predictions of binding affinities when compared to the results obtained using our modified-FF.

We next investigate the effect of ionic concentration on the measured binding free energy and mechanism. **5** is the only ligand in the dataset with experimentally reported binding affinities at both 0 and 50 mM salt concentrations, enabling a direct assessment of salt-dependent effects. The experimental binding affinity of **5** decreases by ~2.2 kcal/mol (Table I) in the presence of a definite salt concentration. Consistent with the experiments, we also observed a decrease of ~2 kcal/mol in binding affinity upon increasing the salt

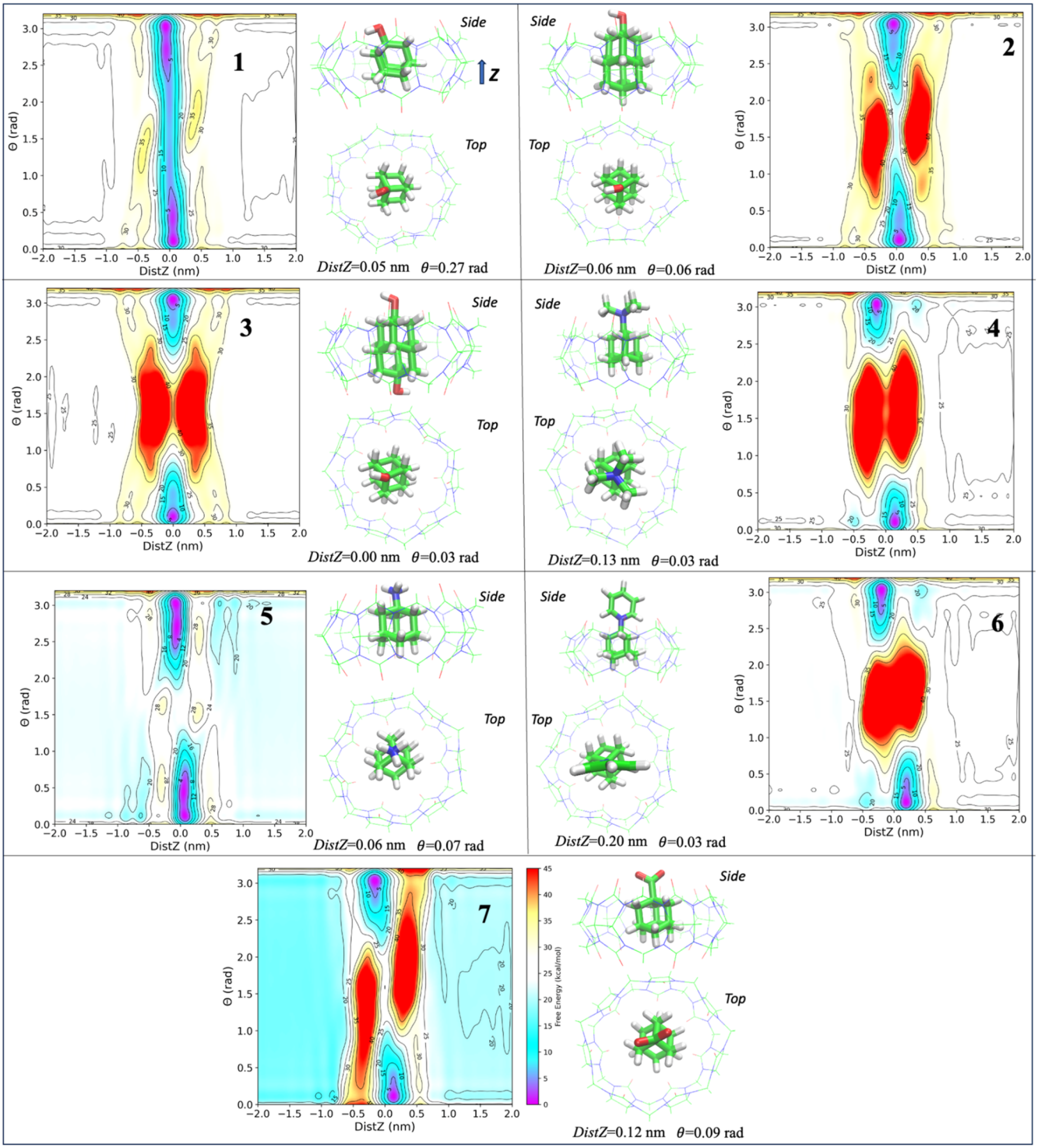

FIG. 3. 2D binding free energy surface of 1–7 as a function of the *DistZ* and θ CVs, calculated using the modified-FF (RESP). The ionic strength is the same as in the experiment.[46–48] The molecule IDs are shown in the inset along with the top and side view of minima state. 1–3 are at 0 mM concentration and 4–7 are at 50 mM concentrations. The color bar shown for molecule 7 applies to all the panels.

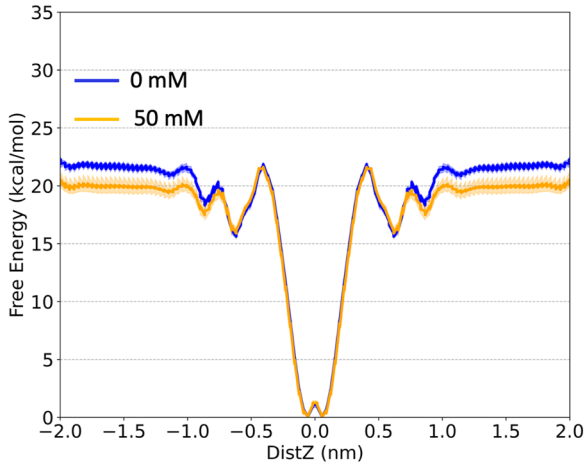

FIG. 4. Free energy profile of ligand **5** as a function of the *DistZ* CV using the GAFF (AM1-BCC) and modified-FF (AM1-BCC), with and without ion concentration effects. The plots are constructed by averaging the free energy over *DistZ* in both the +Z and −Z directions.

concentration from 0 to 50 mM (Fig. 4). A decrease is also observed for all the positively charged and neutral ligands investigated here (Table II and Fig. S13).

In contrast, for the negatively charged ligand **7**, our simulations predicted a moderate increase in binding affinity at higher ionic strength (Fig. S13). In addition, all the force fields predict the same trends with increasing salt concentrations (see Fig. S14, Table S6). The absence of experimental data at different concentrations prevents us from validating this result. A possible explanation for our results is the following: for neutral and positively charged ligands, the presence of Na^+ ions at a definite ionic strength promotes their interaction with the carbonyl portals of CB7, thereby blocking ligand access and weakening the host–guest interaction. Similar explanations have been discussed experimentally, where increased ionic strength reduces the binding affinity of neutral and cationic guests due to competitive interactions at the carbonyl portal sites of CB7.[50,81] In contrast, for the negatively charged ligand (molecule **7**), Na^+ ions reduce the electrostatic repulsion between the ligand's carboxylate group and the carbonyl portals, thereby facilitating binding (discussed in Sec. IX of the supplementary material, Figs. S15 and S16).

TABLE II. Modified-FF (RESP)-based binding free energies for **1–7** at 0 and 50 mM ion concentrations.

	$\Delta G_{bind}^{\{\text{modified-FF(RESP)}\}}$ (kcal/mol)	
Molecule ID	0 mM	50 mM
1	−18.5 ± 0.3	−16.8 ± 0.3
2	−19.9 ± 0.2	−18.0 ± 0.5
3	−19.2 ± 0.2	−16.8 ± 0.1
4	−20.8 ± 0.1	−19.3 ± 0.5
5	−17.9 ± 0.2	−16.2 ± 0.2
6	−20.9 ± 0.1	−18.7 ± 0.1
7	−10.0 ± 0.1	−13.3 ± 1.5

The shape of the free energy surface remains unchanged on passing from *modified-FF* (RESP) to *modified-FF* (AM1-BCC) and GAFF (AM1-BCC)-based calculations (Figs. S13 and S14). This indicates consistent qualitative features.

However, the free energy landscapes differ quantitatively for the adamantane derivatives **1** and **4–7** (Table III). The ligand affinities using the *modified-FF* (RESP) are within ~1.0–2.5 kcal/mol from the experimental values: a significant improvement compared to the predictions of *GAFF* (AM1-BCC) (see Table III), which overestimates them by 9–13 kcal/mol, irrespective of the guest size or charge. This indicates the limited reliability of the *GAFF* (AM1-BCC), which has been discussed previously (Table S1).[31] A comparison with the results obtained using the *modified-FF* (AM1-BCC) shows that re-fitting the LJ parameters alone leads to a consistent improvement across all systems, already reducing the discrepancy with the experiment to 3–7 kcal/mol. Using RESP charges shows further improvement, especially for **4–7** (Table III).

In contrast, the *modified-FF* (RESP) does not lead to a significant improvement for the diamantane-based molecules **2** and **3**. The prediction based on all the FFs used here overestimates binding affinities by ~10 kcal/mol. This suggests that, in these cases, the discrepancy may also be significantly given, at least in part, to by bonded terms.

CONCLUSION

In this work, we demonstrated how our *modified-FF* improves the accuracy of binding free energy for a variety of adamantane

TABLE III. Comparison of binding free energies from modified-FF (RESP), modified-FF (AM1-BCC), and with experimental values at respective ionic strengths (0 mM for 1–3; 50 mM for 4–7).

Molecule ID	$\Delta G_{bind}^{\{\text{Expt}\}}$ (kcal/mol)	$\Delta G_{bind}^{\{\text{modified-FF(RESP)}\}}$ (kcal/mol)	$\Delta G_{bind}^{\{\text{modified-FF(AM1-BCC)}\}}$ (kcal/mol)	$\Delta G_{bind}^{\{\text{GAFF(AM1-BCC)}\}}$ (kcal/mol)
1	−14.1 ± 0.2	−18.5 ± 0.3	−19.6 ± 0.2	−23.8 ± 0.1
2	−9.3 ± 0.4	−19.9 ± 0.2	−19.3 ± 0.2	−22.3 ± 0.1
3	−9.6 ± 0.4	−19.2 ± 0.2	−20.0 ± 0.1	−23.5 ± 0.3
4	−16.7 ± 0.1	−19.3 ± 0.5	−21.0 ± 0.4	−28.1 ± 0.2
5	−17.2 ± 0.1	−16.2 ± 0.2	−21.0 ± 0.2	−25.7 ± 0.2
6	−16.8 ± 0.8	−18.7 ± 0.1	−22.3 ± 0.1	−26.5 ± 0.7
7	−11.6 ± 0.1	−13.3 ± 1.5	−9.8 ± 0.5	−13.8 ± 0.6

ligands binding to CB7. This was established via a comparison with experimental results and with simulations conducted using the standard GAFF parameterization. In addition, our work highlights the influence of ionic concentration on binding affinity: increasing the salt concentration led to reduced binding for hydroxyl-substituted neutral ligands and positively charged guests, while enhancing affinity in the case of negatively charged ligands. Significant discrepancies between the experiment and simulation are still observed for the diamantane derivative, which calls for a further improvement of the force field for this class of ligands.

While writing this paper, a molecular simulation study of the highly similar CB8-based host–guest interaction was reported in ChemRxiv (https://doi.org/10.26434/chemrxiv-2025-1x058-v2). Similar to our work, the study found that using RESP charges improved accuracy. In addition, novel to the literature on CBn modeling, we demonstrate here that improving the LJ parameters also improves accuracy.

SUPPLEMENTARY MATERIAL

The supplementary material includes Tables S1–S5 and Figs. S1–S16. The text provides additional information on the time-evolution of CVs, concentration effects on binding free energy, and convergence plots.

ACKNOWLEDGMENTS

The authors acknowledge the Gauss Centre for Supercomputing e.V. (www.gauss-centre.eu) for funding this project by providing computing time through the John von Neumann Institute for Computing (NIC) on the GCS Supercomputer JUWELS at Jülich Supercomputing Centre (JSC). This work was mainly supported under the Helmholtz Artificial Intelligence Cooperation Unit and Helmholtz Metadata Collaboration (Grant Nos. "AI-Receptor" and "MetaSupra").

AUTHOR DECLARATIONS

Conflict of Interest

The authors have no conflicts to disclose.

Author Contributions

A.V. performed all the metadynamics calculations and contributed to the writing of the manuscript. G.S. performed the RESP calculations and contributed to the writing. D.M., P.C., G.R., and F.B. conceived the project and contributed to the writing.

Amal Vijay: Conceptualization (equal); Data curation (equal); Formal analysis (equal); Investigation (equal); Methodology (equal); Resources (equal); Visualization (equal); Writing – original draft (equal); Writing – review & editing (equal). **Giacomo Salvadori**: Data curation (equal); Investigation (equal); Methodology (equal); Writing – review & editing (equal). **Frank Biedermann**: Conceptualization (equal); Funding acquisition (equal); Writing – review & editing (equal). **Giulia Rossetti**: Conceptualization (equal); Formal analysis (equal); Funding acquisition (equal); Investigation (equal); Methodology (equal); Project administration (equal); Resources (equal); Supervision (equal); Writing – review & editing (equal). **Paolo Carloni**: Conceptualization (equal); Formal analysis (equal); Funding acquisition (equal); Investigation (equal); Methodology (equal); Project administration (equal); Resources (equal); Supervision (equal); Writing – review & editing (equal). **Davide Mandelli**: Conceptualization (equal); Formal analysis (equal); Funding acquisition (equal); Investigation (equal); Methodology (equal); Project administration (equal); Resources (equal); Supervision (equal); Writing – review & editing (equal).

DATA AVAILABILITY

The data that support the findings of this study are available from the corresponding authors upon reasonable request.

ABBREVIATIONS

MSR	metabolite binding synthetic receptor
LJ	Lennard-Jones
CBn	Cucurbit[n]uril
CB7	Cucurbit[7]uril
CV	collective variable
COM	center of mass
MD	molecular dynamics
GAFF	general AMBER force field

REFERENCES

[1] W. Xue, P. Y. Zavalij, and L. Isaacs, Angew. Chem., Int. Ed. **59**, 13313 (2020).
[2] L. Cao *et al.*, Angew. Chem., Int. Ed. **53**, 988 (2014).
[3] L. M. Grimm *et al.*, ChemistryEurope **2**, e202400003 (2024).
[4] W. S. Jeon *et al.*, J. Am. Chem. Soc. **127**, 12984 (2005).
[5] M. Chvojka, H. Valkenier, and V. Šindelář, Org. Chem. Front. **12**, 130 (2025).
[6] S. Sarkar *et al.*, Angew. Chem., Int. Ed. **62**, e202214705 (2023).
[7] A. S. Braegelman and M. J. Webber, Theranostics **9**, 3017 (2019).
[8] N. Barooah, J. Mohanty, and A. C. Bhasikuttan, Langmuir **38**, 6249 (2022).
[9] F. Y. Chen *et al.*, Angew. Chem., Int. Ed. **64**(29), e202500916 (2025).
[10] J. Krämer *et al.*, Chem. Rev. **122**, 3459 (2022).
[11] J. Krämer *et al.*, Nat. Commun. **14**, 518 (2023).
[12] B. Gong *et al.*, J. Am. Chem. Soc. **137**, 8908 (2015).
[13] Y.-L. Ma *et al.*, CCS Chem. **4**, 1977 (2022).
[14] K. L. Liu, Z. Zhang, and J. Li, Soft Matter **7**, 11290 (2011).
[15] J. Jin *et al.*, J. Mater. Chem. B **7**, 1637 (2019).
[16] E. A. Appel *et al.*, J. Am. Chem. Soc. **132**, 14251 (2010).
[17] A. Harada, Y. Takashima, and M. Nakahata, Acc. Chem. Res. **47**, 2128 (2014).
[18] M. Yan *et al.*, Adv. Mater. **36**, 2304249 (2024).
[19] S. J. Barrow *et al.*, Chem. Rev. **115**, 12320 (2015).
[20] K. I. Assaf and W. M. Nau, Chem. Soc. Rev. **44**, 394 (2015).
[21] J. W. Lee *et al.*, Acc. Chem. Res. **36**, 621 (2003).
[22] S. Sinn and F. Biedermann, Isr. J. Chem. **58**, 357 (2018).
[23] M. Aleśković and M. Šekutor, RSC Med. Chem. **15**, 433 (2024).
[24] V. Limongelli, M. Bonomi, and M. Parrinello, Proc. Natl. Acad. Sci. U. S. A. **110**, 6358 (2013).
[25] J. Setiadi *et al.*, Angew. Chem., Int. Ed. **64**, e202505713 (2025).
[26] J. Wang *et al.*, J. Comput. Chem. **25**, 1157 (2004).
[27] K. Vanommeslaeghe *et al.*, J. Comput. Chem. **31**, 671 (2009).

[28]W. L. Jorgensen, D. S. Maxwell, and J. Tirado-Rives, J. Am. Chem. Soc. **118**, 11225 (1996).
[29]S. Boothroyd *et al.*, J. Chem. Theory Comput. **19**, 3251 (2023).
[30]Y. Qiu *et al.*, J. Chem. Theory Comput. **17**, 6262 (2021).
[31]H. S. Muddana *et al.*, J. Comput.-Aided Mol. Des. **28**, 305 (2014).
[32]M. Amezcua, L. El Khoury, and D. L. Mobley, J. Comput.-Aided Mol. Des. **35**, 1 (2021).
[33]J. Yin *et al.*, J. Comput.-Aided Mol. Des. **31**, 1 (2016).
[34]W. L. Jorgensen *et al.*, J. Chem. Phys. **79**, 926 (1983).
[35]L.-P. Wang, T. J. Martinez, and V. S. Pande, J. Phys. Chem. Lett. **5**, 1885 (2014).
[36]H. J. C. Berendsen, J. R. Grigera, and T. P. Straatsma, J. Phys. Chem. **91**, 6269 (2002).
[37]S. Izadi and A. V. Onufriev, J. Chem. Phys. **145**, 074501 (2016).
[38]K. Gao *et al.*, J. Chem. Theory Comput. **11**, 4555 (2015).
[39]P. Febrer Martinez *et al.*, J. Chem. Theory Comput. **20**, 10275 (2024).
[40]D. Shetty *et al.*, Chem. Soc. Rev. **44**, 8747 (2015).
[41]S. He *et al.*, Nat. Chem. **10**, 1252 (2018).
[42]P. S. Hudson *et al.*, J. Chem. Theory Comput. **14**, 6327 (2018).
[43]P. S. Hudson *et al.*, J. Comput.-Aided Mol. Des. **32**, 983 (2018).
[44]D. González *et al.*, J. Chem. Inf. Model. **62**, 4162 (2022).
[45]P. Raiteri *et al.*, J. Phys. Chem. B **110**, 3533 (2006).
[46]S. Moghaddam *et al.*, J. Am. Chem. Soc. **133**, 3570 (2011).
[47]L. M. Grimm *et al.*, Chem. - Eur. J. **28**, e202200529 (2022).
[48]S. Liu *et al.*, J. Am. Chem. Soc. **127**, 15959 (2005).
[49]A. J. Selinger and D. H. Macartney, RSC Adv. **7**, 42513 (2017).
[50]A. Buczkowski, J. Mol. Liq. **345**, 117857 (2022).
[51]M. D. Hanwell *et al.*, J. Cheminf. **4**, 17 (2012).
[52]J. M. Turney *et al.*, Wiley Interdiscip. Rev.:Comput. Mol. Sci. **2**, 556 (2011).
[53]J. Wang *et al.*, J. Mol. Graphics Modell. **25**, 247 (2006).
[54]A. Jakalian, D. B. Jack, and C. I. Bayly, J. Comput. Chem. **23**, 1623 (2002).
[55]L. Kagami *et al.*, Bioinformatics **39**, btad350 (2023).
[56]X. He *et al.*, J. Chem. Phys. **153**, 114502 (2020).
[57]D. J. Cole *et al.*, J. Chem. Theory Comput. **12**, 2312 (2016).
[58]T. Verstraelen *et al.*, J. Chem. Theory Comput. **12**, 3894 (2016).
[59]C. Ringrose *et al.*, Phys. Chem. Chem. Phys. **24**, 17014 (2022).
[60]J. T. Horton *et al.*, J. Chem. Inf. Model. **59**, 1366 (2019).
[61]A. Tkatchenko and M. Scheffler, Phys. Rev. Lett. **102**, 073005 (2009).
[62]C. I. Bayly *et al.*, J. Phys. Chem. **97**, 10269 (2002).
[63]G. Scalmani and M. J. Frisch, J. Chem. Phys. **132**, 114110 (2010).
[64]J. Tomasi, B. Mennucci, and R. Cammi, Chem. Rev. **105**, 2999 (2005).
[65]E. Cancès, B. Mennucci, and J. Tomasi, J. Chem. Phys. **107**, 3032 (1997).
[66]A. L. Hickey and C. N. Rowley, J. Phys. Chem. A **118**, 3678 (2014).
[67]I. S. Joung and T. E. Cheatham, J. Phys. Chem. B **112**, 9020 (2008).
[68]U. Essmann *et al.*, J. Chem. Phys. **103**, 8577 (1995).
[69]B. Hess *et al.*, J. Comput. Chem. **18**, 1463 (1997).
[70]G. Bussi, D. Donadio, and M. Parrinello, J. Chem. Phys. **126**, 014101 (2007).
[71]H. J. C. Berendsen *et al.*, J. Chem. Phys. **81**, 3684 (1984).
[72]M. Parrinello and A. Rahman, J. Appl. Phys. **52**, 7182 (1981).
[73]Y.-W. Hsiao and P. Söderhjelm, J. Comput.-Aided Mol. Des. **28**, 443 (2014).
[74]A. Barducci, G. Bussi, and M. Parrinello, Phys. Rev. Lett. **100**, 020603 (2008).
[75]G. A. Tribello *et al.*, Comput. Phys. Commun. **185**, 604 (2014).
[76]M. J. Abraham *et al.*, SoftwareX **1–2**, 19 (2015).
[77]Z. Sun *et al.*, J. Chem. Inf. Model. **61**, 6107 (2021).
[78]X. Liu *et al.*, Molecules **28**, 2767 (2023).
[79]Z. Sun and P. Procacci, Phys. Chem. Chem. Phys. **26**, 19887 (2024).
[80]Z. Sun *et al.*, Molecules **28**, 3124 (2023).
[81]W. Ong and A. E. Kaifer, J. Org. Chem. **69**, 1383 (2004).